Biochemical and Biophysical Research Communications 447 (2014) 32–37

Contents lists available at ScienceDirect

Biochemical and Biophysical Research Communications

journal homepage: www.elsevier.com/locate/ybbrc

Crystal structure of glycoside hydrolase family 127 β-L-arabinofuranosidase from *Bifidobacterium longum*

Tasuku Ito [a,1], Kyo Saikawa [a,1], Seonah Kim [b,1], Kiyotaka Fujita [c], Akihiro Ishiwata [d], Sophon Kaeothip [e], Takatoshi Arakawa [a], Takayoshi Wakagi [a], Gregg T. Beckham [b,*], Yukishige Ito [d,e], Shinya Fushinobu [a,*]

[a] Department of Biotechnology, The University of Tokyo, Tokyo, Japan
[b] National Bioenergy Center, National Renewable Energy Laboratory, Golden, CO, USA
[c] Faculty of Agriculture, Kagoshima University, Korimoto, Kagoshima, Japan
[d] Synthetic Cellular Chemistry Laboratory, RIKEN, Japan
[e] ERATO Glycotrilogy Project, JST, Wako, Saitama, Japan

ARTICLE INFO

Article history:
Received 7 March 2014
Available online 27 March 2014

Keywords:
Crystal structure
Quantum mechanical calculations
Retaining glycoside hydrolase
DUF1680
Plant polysaccharide
Human gut bacteria

ABSTRACT

Enzymes acting on β-linked arabinofuranosides have been unknown until recently, in spite of wide distribution of β-L-arabinofuranosyl oligosaccharides in plant cells. Recently, a β-L-arabinofuranosidase from the glycoside hydrolase family 127 (HypBA1) was discovered in the newly characterized degradation system of hydroxyproline-linked β-L-arabinooligosaccharides in the bacterium *Bifidobacterium longum*. Here, we report the crystal structure of HypBA1 in the ligand-free and β-L-arabinofuranose complex forms. The structure of HypBA1 consists of a catalytic barrel domain and two additional β-sandwich domains, with one β-sandwich domain involved in the formation of a dimer. Interestingly, there is an unprecedented metal-binding motif with Zn^{2+} coordinated by glutamate and three cysteines in the active site. The glutamate residue is located far from the anomeric carbon of the β-L-arabinofuranose ligand, but one cysteine residue is appropriately located for nucleophilic attack for glycosidic bond cleavage. The residues around the active site are highly conserved among GH127 members. Based on biochemical experiments and quantum mechanical calculations, a possible reaction mechanism involving cysteine as the nucleophile is proposed.

1. Introduction

α-L-Arabinofuranosidases have been extensively studied, and they are found in several glycoside hydrolase (GH) families [1]. In contrast, β-L-arabinofuranosidases (β-AFases) have been discovered only recently and no structural studies are available. β-L-Arabinofuranoside (β-Ara*f*) residues have been found in plant hydroxyproline (Hyp)-rich glycoproteins (HPRGs) such as extensins and solanaceous lectins [2,3]. HPRGs are widely observed in plant cell walls and are essential in root hair growth [4]. β-Ara*f*-containing HPRGs have repetitive Ser-Hyp_4 motifs and the majority of the Hyp-*O*-linked arabinofuranosides are Ara*f*-α1,3-Ara*f*-β1,2-Ara*f*-β1,2-Ara*f*β-Hyp (Ara_4-Hyp) and Ara*f*-β1,2-Ara*f*-β1,2-Ara*f* β-Hyp (Ara_3-Hyp) [5]. Moreover, terminal β-Ara*f*s are found in many plant biopolymers [6] and plant glycopeptide hormones [7]. Recently, β-Ara*f*s in plants have been shown to play essential roles in both vegetative and reproductive growth [8].

In 2011, Fujita et al. discovered an Ara_4-Hyp degradation system from the human gut commensal bacterium, *Bifidobacterium longum* [9]. The gene cluster consists of one ABC-type sugar transporter, two extracellular enzymes and one intracellular enzyme. One of the two extracellular enzymes is a GH121 β-L-arabinobiosidase HypBA2 that releases Ara*f*-β1,2-Ara*f* (β-Ara_2) from Ara_3-Hyp. The intracellular enzyme is a GH127 β-AFase HypBA1 (EC 3.2.1.185), which can act on the terminal β-Ara*f* of β-Ara_2, Ara_2-Hyp, and Ara-Hyp [10]. HypBA1 catalyzes transglycosylation with Ara_2-Hyp and 1-alkanols. The reaction product from methanol was determined to be methyl-β-Ara*f* and was hydrolyzed by HypBA1, indicating that HypBA1 is a retaining GH. To date, the GH127 family has approximately 350 members mainly from bacteria, which have been grouped into a wider Pfam family, domain of unknown function (DUF) 1680. The DUF1680 family has approximately 600 members and is distributed among more than 300 organisms including plant pathogenic bacteria, enteric bacteria,

* Corresponding authors. Address: Department of Biotechnology, The University of Tokyo, 1-1-1 Yayoi, Bunkyo-ku, Tokyo 113-8657, Japan. Fax: +81 3 5841 5151 (S. Fushinobu).
E-mail addresses: Gregg.Beckham@nrel.gov (G.T. Beckham), asfushi@mail.ecc.u-tokyo.ac.jp (S. Fushinobu).
[1] These authors contributed equally to this work.

http://dx.doi.org/10.1016/j.bbrc.2014.03.096
0006-291X/

fungi, and plants, suggesting that GH127 β-AFases and their homologs in DUF1680 are involved in remodeling and degradation of plant cell walls.

A preliminary crystallographic study of HypBA1 has been reported very recently [11], but its structural analysis is not yet published. Moreover, no crystal structures of proteins belonging to GH127 or DUF1680 are available. In this study, we report the crystal structure of HypBA1 from *B. longum* JCM1217 (BLLJ_0211), which is a three-dimensional structure of enzyme acting on a β-L-arabinofuranosidic bond. Based on biochemical, structural, and computational analyses, we propose a possible reaction mechanism of GH127 β-AFases, in which a cysteine residue acts as a nucleophile.

2. Materials and methods

2.1. Protein production, purification and crystallography

The C-terminally $(His)_6$-tagged HypBA1 was overexpressed as described previously [10]. *Escherichia coli* C43 (DE3) and B834 (DE3) were used for native and selenomethionine-labeled protein expressions, respectively. The transformants were cultured in Luria–Bertani medium (native protein) or LeMaster medium (selenomethionine-labeled protein) containing 100 mg/L ampicillin at 37 °C for 5 h. Isopropyl 1-thio-β-D-galactopyranoside was added to a final concentration of 1.0 mM. Following an additional incubation at 25 °C for 20 h, the cells were harvested by centrifugation and suspended in 50 mM Tris–HCl (pH 7.5). After sonication and centrifugation to remove cell debris, the protein was purified to homogeneity by column chromatography using Ni–NTA superflow (QIAGEN) and Superdex 200 pg 16/60 (GE Healthcare). For biochemical analysis, the protein was overexpressed by cultures supplemented with 0.5 mM $ZnSO_4$.

Crystals of native HypBA1 in ligand-free native form and ligand-free selenomethionine-labeled form were obtained at 20 °C using the hanging drop vapor diffusion method by mixing 1.0 μL of protein solution containing 19.5 mg/mL with an equal volume of a reservoir solution, which contained 0.9 M sodium citrate and 0.1 M Na-cacodylate (pH 6.5) for the ligand-free form, or 0.7 M sodium citrate and 0.1 M MES–NaOH (pH 6.5) for the selenomethionine-labeled form. For cryoprotectant, 20% glycerol (ligand-free form) or 20% trehalose (selenomethionine-labeled) was used. Crystals complexed with arabinose were obtained with a protein solution of 45 mg/mL, and a reservoir solution of 0.7 M sodium citrate, 0.1 M MES–NaOH (pH 6.5), 10 mM dithiothreitol (DTT), and 20% L-arabinose. The crystals were flash-cooled in a nitrogen stream at 100 K. Diffraction data were collected at the Photon Factory of the High Energy Accelerator Research Organization (KEK, Tsukuba, Japan) and at SPring-8 (Nishi-Harima, Japan). Programs used for crystallography are described in Supplementary methods. The statistics for data collection and refinement are provided in Table S1. The coordinates and structure factors have been deposited in the PDB under accession codes 3WKW and 3WKX.

2.2. Mutagenesis and biochemical analysis

The E322A and E338A mutants were constructed as described previously [10]. Other mutants were constructed via site directed mutagenesis by the overlap extension method with primers listed in Table S2. Activity on *p*-nitrophenyl-β-L-Ara*f* was measured as described previously [12]. The standard assay mixture (100 μL) consisted of 50 mM sodium acetate buffer (pH 4.5), 10 mM DTT, 0.05–0.5 mM *p*-nitrophenyl-β-Ara*f*, and the enzyme. The assays were initiated by addition of 0.05 mg/mL (WT) or >1.0 mg/ml (mutants) enzyme (5 μL), which was preincubated with 10 mM DTT at 37 °C for 30 min. For metal content analysis, the protein sample (1 mg) was dried at 90 °C for 15 h, subsequently dissolved in 13 N HNO_3 (30 μL), and then heated at 90 °C overnight. After drying, it was dissolved with 0.1 N HNO_3. The metal contents of the protein were measured with an inductively coupled plasma–optical emission spectrometer (ICP–OES) SII SPS3500 (Seiko Instruments Inc.).

2.3. Quantum mechanical calculations

Density functional theory (DFT) calculations were performed with Gaussian09 [13] on an active site model (ASM) of HypBA1, which includes the residues His142, His194, His270, Glu322, Glu338, Cys340, Tyr386, Cys415, Cys417, Cys418, and Zn^{2+}. Smaller and larger ASM were examined to select the optimal ASM using DFT geometry optimizations and the best ASM was chosen here based on shape and electronic properties compared to the experimental structure. All geometry optimizations were conducted using the hybrid GGA B3LYP functional with the 6-31G(d) basis set for all atoms and single point energies were computed on all optimized geometries with the large 6-311++G(d,p) basis set. Harmonic vibrational frequencies were computed for all optimized structures to verify that they were either minima or transition structures, possessing zero imaginary frequencies or one imaginary frequency, respectively. The conductor-like polarizable continuum model [14,15] using diethyl either solvation ($\varepsilon = 4$) [16] was applied in all our calculations to mimic the protein environment. The positions of all α- and β-carbons of amino acid residues were fixed during geometry optimizations to keep the position of backbone structure, while rest of the ASM is fully optimized. We report ΔE for the system energies due to imposing Cartesian constraints. Intrinsic reaction coordinate calculations are not possible for the ASM because of the Cartesian constraints. Thus, we displaced each transition state by a small fraction (0.2) of the imaginary normal mode vibration and performed full geometry optimizations [17,18], which confirmed each transition state connected the energy minima of each of the reaction coordinates.

3. Results and discussion

3.1. Overall structure

Ligand-free and arabinose complex structures of HypBA1 containing one molecule in the asymmetric unit were determined at 2.2 Å and 2.0 Å resolution, respectively. The monomer consists of three domains (Fig. 1A, arabinose complex): a catalytic $(\alpha/\alpha)_6$ barrel domain (residues 1–432, gray), β-sandwich domain 1 (residues 433–540, blue), and β-sandwich domain 2 (541–659, green). The catalytic domain is structurally similar to several other, unrelated carbohydrate-active enzymes from different GH families (Table S3). The β-sandwich domain 1 shows a similarity to C-terminal domains of GH44, GH27, and GH39 enzymes. The β-sandwich domain 2 is somewhat similar to the N-terminal domain of ErbB4 kinase and is involved in formation of a dimer, which is created by a crystallographic 2-fold axis (Fig. 1B). The molecular masses of the HypBA1 as deduced from the amino acid sequence, estimated by SDS–PAGE, and calibrated gel filtration chromatography are 74.4, 75.4, and 140.6 kDa, respectively, suggesting that the enzyme is dimeric in solution.

3.2. Active site

Fig. 1C and D show the active site in the ligand-free and arabinose complex structures. In our previous report, Glu322 and Glu338 were identified as critical residues for catalytic activity

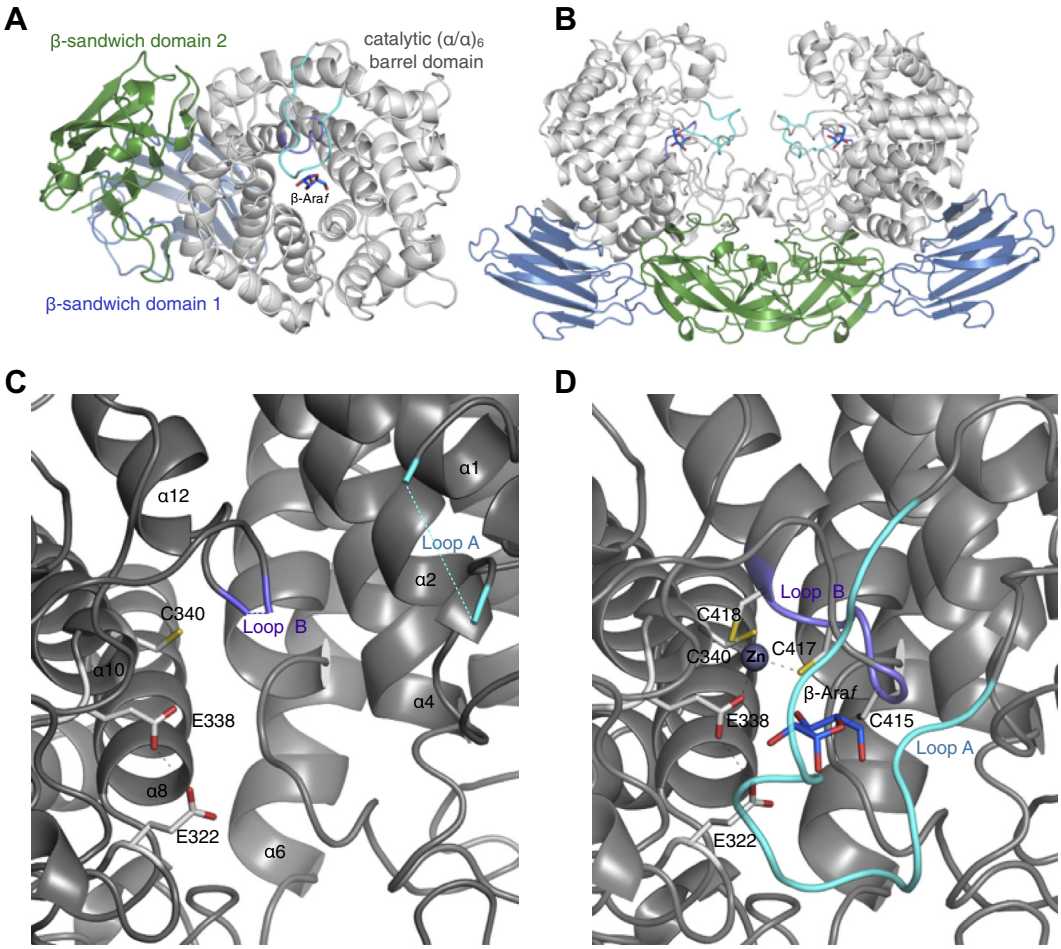

Fig. 1. Structure of HypBA1. (A) Monomer and (B) dimer structures of the L-arabinose complex. The catalytic $(\alpha/\alpha)_6$ barrel, β-sandwich 1, and β-sandwich 2 domains are shown in gray, blue, and green, respectively. (C) The ligand-free active site exhibiting two disordered loops. (D) The arabinose-complex structure has a β-L-arabinofuranose molecule in the active site. Both Loop A (cyan) and Loop B (purple) are ordered in the complex structure.

[10]. Glu322 is located on a loop connecting α9 and α10, and Glu338 is located at the N-terminus of α10. In the ligand-free structure, the two loops are disordered (Fig. 1C). Loop A (residues 35–48, cyan) is located after an external helix α1, and this region shows low conservation among the GH127 family (Fig. 2A). Loop B (414–418, purple) is located near the two Glu residues at the N-terminal end of the sixth inner helix α12. The Loop B region contains three Cys residues and is highly conserved among GH127 family members (Fig. 2A).

Crystals for the arabinose (product) complex structure were prepared by co-crystallization in the presence of a reducing agent (DTT) and L-arabinose. A clear electron density for a β-L-arabinofuranoside molecule was observed at the active site (Fig. 2B) although this form of L-arabinose is minor in solution compared with α-pyranose, β-pyranose, and α-furanose [19]. The sugar ring of β-L-arabinofuranoside adopts a relaxed $^2T_3$ conformation. In the arabinose complex structure, both Loop A and Loop B are clearly observed (Fig. 1D). Loop A covers the barrel and completely shields the active site from the solvent. The C-terminal half of Loop B forms a helix connected to α12. Interestingly, a strong metal peak was observed at the center of two cysteines in Loop B (Cys417 and Cys418), and Cys340 and Glu338 in a neighboring helix α10 (Fig. S1). To identify the metal peak, we measured the metal content of a purified HypBA1 protein sample. Zn contents of the enzyme purified from *E. coli* cultures without Zn supplementation varied lot-by-lot in a range of 0.21–0.69 mol per mol protein, but other metals, including Fe, Ni, Mn, Co, Ca, Mg, and Cu were not detected (<0.03 mol per mol protein). When the sample was prepared from cultures supplemented with 0.5 mM $ZnSO_4$, 1.06 mol per mol protein of Zn was detected (Table 1). Crystallographic anomalous scattering analysis was conducted, and a Bijvoet difference density map of the data collected at 1.280 Å wavelength exhibits a strong peak at the metal site (Fig. 2B), whereas a difference map of the data collected at 1.300 Å wavelength, which is above the absorption edge of Zn (1.2837 Å), shows a greatly reduced anomalous scattering ability. Therefore, a Zn^{2+} ion was modeled at this site. The temperature factor of the Zn^{2+} after the refinement is 30.7 $Å^2$, which is comparable to the average temperature factor of waters in the crystal structure (40.1 $Å^2$). Coordination of the Zn^{2+} ion is near perfectly tetrahedral, and the distance to the Cys417 Sγ atom (2.4 Å) is slightly longer than those to the other three ligand atoms (2.1–2.2 Å).

3.3. Biochemical and mutational analyses

Very recently, we established a synthetic route to produce a chromogenic synthetic substrate, *p*-nitrophenyl-β-L-Ara*f*, on which HypBA1 exhibits substantial activity [12]. The K_m, k_{cat}, and k_{cat}/K_m values of HypBA1 against *p*-nitrophenyl-β-Ara*f* were 0.13 mM, 16.6 s^{-1}, and 130 s^{-1} mM^{-1}, respectively. By using this synthetic substrate, we examined effects of reducing agents, Zn^{2+}, EDTA, and thiol modifiers on the activity of HypBA1 against

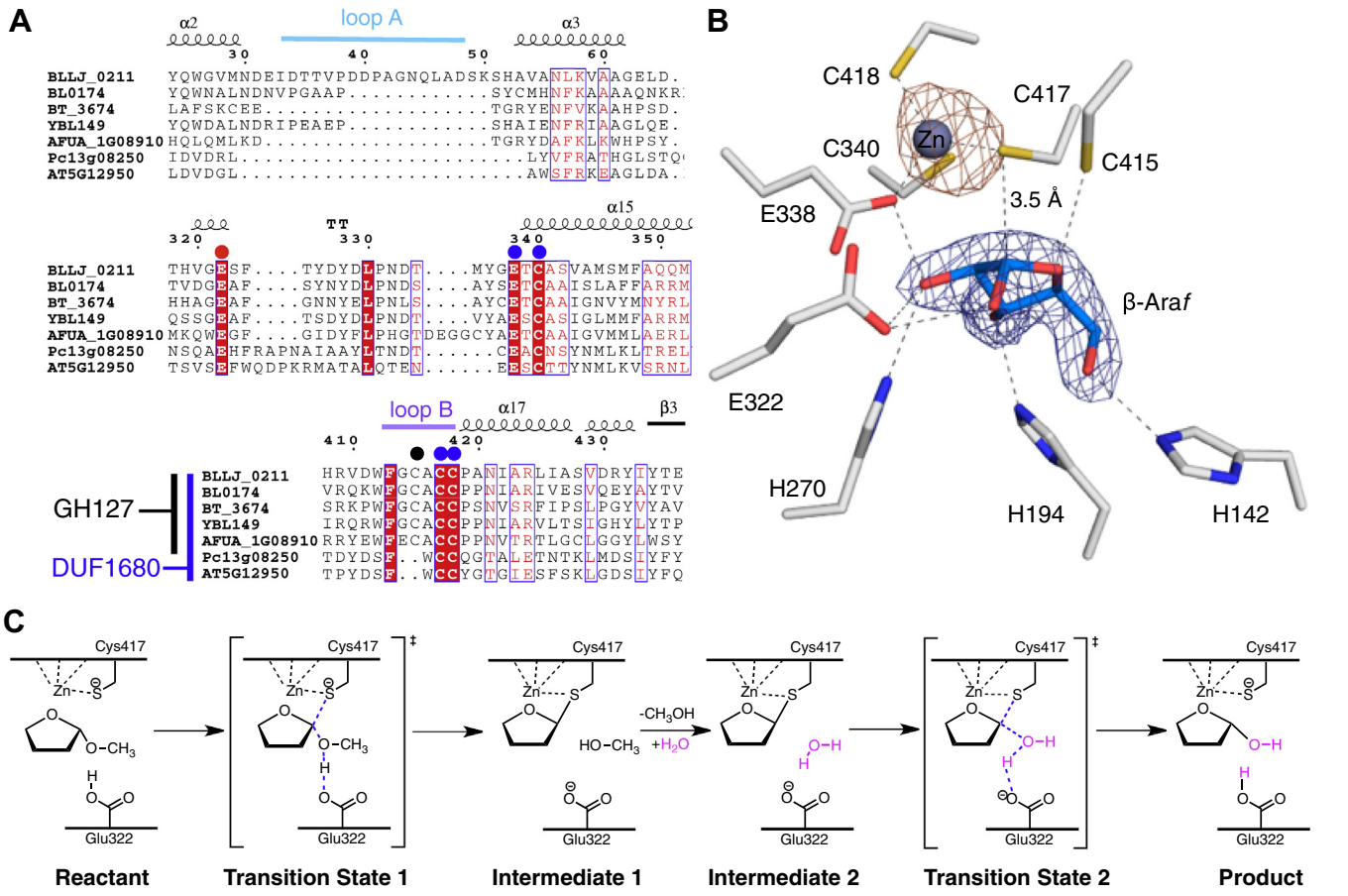

Fig. 2. Sequence details, active center, and proposed catalytic mechanism for HypBA1. (A) Multiple sequence alignment of DUF1680 members. The catalytic acid/base catalyst Glu322, residues coordinating Zn^{2+} (Glu338, Cys340, Cys417 and Cys418), and Cys415 are marked with red, blue and black marks, respectively. The sequences are labeled with the genome locus tags, and their source organisms are as follows: BLLJ_0211, *B. longum* JCM1217; BL0174; *B. longum* NCC2705; BT_3674; *Bacteroides thetaiotaomicron*; YBL149; *Escherichia coli* BL21 (DE3); AFUA_1G08910; *Aspergillus fumigatus*; Pc13g08250; *Penicillium chrysogenum*; AT5G12950; *Arabidopsis thaliana*. The first five sequences are included in GH127 but the latter two are not. (B) The HypBA1 active site. $|F_o| - |F_c|$ omit electron density map (contoured at 1.5σ) for β-L-arabinofuranose and the anomalous difference density map of the data collected at a wavelength of 1.280 Å (contoured at 10σ) are shown as blue and brown meshes, respectively. (C) Proposed reaction mechanism.

Table 1
Zn contents and catalytic activities of wild-type and mutants of HypBA1.

	Zn content (mol/mol protein)	Specific activity (U/mg)[a]
Wild type	1.06 ± 0.01	9.21 ± 0.40
E322Q	0.643	0.013 ± 0.001
E322A	0.813	(4.2×10^{-4})
E338Q	0.491	(1.7×10^{-4})
E338A	0.145	(1.3×10^{-4})
C340S	0.443	(1.3×10^{-4})
C340A	0.075	(5.4×10^{-4})
C415S	0.830	0.29 ± 0.02
C415A	0.838	0.52 ± 0.04
C417S	0.286	ND[b]
C417A	0.112	ND[b]
C418S	0.085	(1.3×10^{-3})
C418A	0.091	(1.7×10^{-4})

[a] Activities of *p*-nitrophenyl-β-L-Ara*f* hydrolysis (0.2 mM) were measured in 50 mM Na-acetate (pH 4.5) and 10 mM DTT at 37 °C. Detectable but weak activities (<0.01 U/mg) are shown in parentheses.
[b] Not detected ($<1 \times 10^{-5}$ U/mg).

p-nitrophenyl-β-Ara*f* (Table S4). Addition of reducing agents increased the activity, which is consistent with our previous report [10]. We speculate that this result indicates a fraction of the enzyme preparation included incorrectly connected disulfide bonds around the active site. HypBA1 was slightly inhibited in the presence of EDTA, indicating a strong Zn^{2+} binding in the active site, and addition of $ZnCl_2$ did not increase the activity. Notably, the activity was strongly inhibited in the presence of thiol modifiers, suggesting a crucial role for cysteine residues in catalysis.

The active site structure of the arabinose complex is shown in Fig. 2B. All of the hydroxyl groups of β-L-arabinofuranoside form direct hydrogen bonds to protein atoms. Two glutamate residues (Glu322 and Glu338) and three histidine residues (His142, His194, and His270) are involved in substrate recognition. Because the catalytically critical Glu322 forms a hydrogen bond with the O1 hydroxyl, this residue is assigned as the catalytic acid/base residue. The space towards Loop A near the O1 hydroxyl of the β-L-arabinofuranoside ligand forms a pocket of 1364 $Å^3$, which probably corresponds to the positive subsites or the aglycone binding site. The other important Glu residue, Glu338, forms a hydrogen bond with the O2 hydroxyl and is distantly located to the anomeric carbon atom of β-L-arabinofuranoside (Glu338 Oε2–C1 distance = 4.2 Å). Unexpectedly, one of the Zn^{2+}-coordinating cysteines, Cys417, is close to the anomeric carbon (3.5 Å) with a three-dimensional configuration suitable for an in-line nucleophilic attack (Cys417 Sγ–C1–O1 angle = 158.4°). The Sγ atom of Cys415 is located 3.4 Å from the O5 atom of β-L-arabinofuranoside. An amino acid sequence alignment shows that residues

corresponding to Glu322 and the Zn^{2+}-coordinating residues are completely conserved in all DUF1680 members (Fig. 2A). However, Cys415 and the three histidines show relatively low conservation in DUF1680 members not included in GH127 (Fig. S2).

To examine the function of the residues in the active site, we performed a mutational analysis by mutating each residue to alanine and to an isosteric amino acid (Table 1). Mutations at the Zn^{2+}-coordinating residues reduced the Zn^{2+} content, whereas mutations at other residues had less effect. For the catalytic activity, the Cys415 mutants retained activity. The K_m, k_{cat}, and k_{cat}/K_m values of C415S and C415A were 0.62 ± 0.14 mM, 1.5 ± 0.2 s^{-1}, and 2.4 s^{-1} mM^{-1}, and 0.42 ± 0.10 mM, 1.8 ± 0.2 s^{-1}, and 4.3 s^{-1} mM^{-1}, respectively, resulting in significant decrease of the k_{cat} value and increase of the K_m value. Mutants at Glu322, Glu338, Cys340, and Cys418 showed very weak but detectable activity. Importantly, mutations of Cys417 completely abolished activity, suggesting that it is an essential residue in the active site.

3.4. Comparison with other enzymes

The catalytically important residues of HypBA1 are all located at the N-terminal side of the fifth (Glu322, Glu338, and Cys340) and the sixth (Cys417 and Cys418) inner helices. The catalytic domain of HypBA1 shows significant structural similarities to several GH enzymes (Table S2), but none of them exhibit catalytic residues at a similar position to HypBA1. The catalytic residues of GH88, GH105, and GH126 are located at the N-termini of the first and third inner helices [20–22]. Other $(\alpha/\alpha)_6$ barrel-containing GH families have the catalytic residues at the N-termini of the third and sixth inner helices, or the first and fourth inner helices in circular permutated cases [23]. Interestingly, the Cys_3 + Glu type Zn^{2+}-coordination of HypBA1 is an unprecedented case in metalloproteins. Mononuclear Zn-thiolate sites found in protein structures have been limited to Cys_4, Cys_3 + His, Cys_2 + His_2, Cys_2 + His, Cys + His_2, Cys + His + Asp, or Cys + His + Glu types [24].

3.5. Possible reaction mechanism and quantum mechanical calculations

Based on these data, we tentatively propose a two-step, retaining mechanism for hydrolysis in HypBA1 (Fig. 2C) wherein the nucleophile, Cys417, attacks the anomeric C1 carbon atom of the β-L-arabinofuranosidic bond. The Zn^{2+}-coordination is hypothesized to reduce the pK_a of the Cys417 thiol side chain to aid in nucleophilic attack. During the first glycosylation step, Glu322 acts as the catalytic acid by donating a proton to the glycosidic bond oxygen. The hypothetical *S*-glycosyl-enzyme covalent intermediate then undergoes nucleophilic attack by a water molecule after the product in the +1 subsite is released, which is activated by Glu322 acting as the catalytic base in the deglycosylation step. To ascertain if this proposed reaction mechanism is chemically and thermodynamically plausible, we performed quantum mechanical calculations with an ASM of HypBA1 for both the glycosylation and deglycosylation steps with a methyl-β-Ara*f* substrate as HypBA1 is able to catalytically cleave the glycosidic bond in this substrate [10]. The molecular snapshots for the overall reaction are shown in Fig. 3A. The potential energy landscape of the overall reaction suggests a barrier of 23.2 kcal/mol and

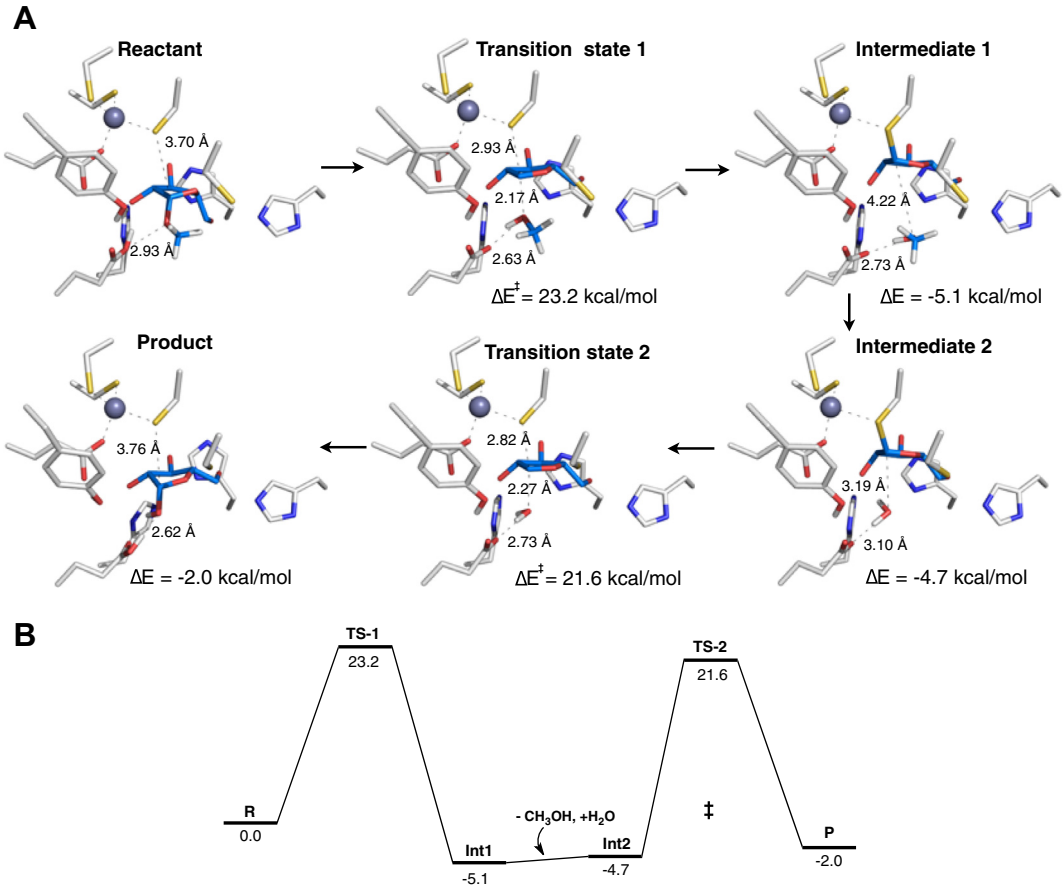

Fig. 3. Quantum mechanical calculations along the proposed HypBA1 reaction pathway. (A) Snapshots of the active site model geometry along the reaction pathway are shown in stick format with the substrate carbon atoms in blue, the enzyme residue carbon atoms in gray, and the Zn^{2+} ion as a gray sphere. (B) The potential energy surface for the HypBA1 chemical reaction.

21.6 kcal/mol for the first and second steps, respectively with an overall potential energy change of −2.0 kcal/mol from reactants to products (Fig. 3B). This suggests that the potential energy barrier, at least for this substrate, is approximately similar in both steps. Importantly, the quantum mechanical calculations demonstrate that the energy barriers for both steps are reasonable for the proposed mechanism, thus lending more credibility to the proposed reaction mechanism for GH127 enzymes through a novel *S*-glycosyl enzyme intermediate.

GHs typically exhibit carboxylate pairs for catalysis, and only a few examples have been found that do not follow this paradigm [25,26]. On the other hand, proteases (peptidases) constitute another major enzyme class of hydrolases that employ a much broader variety of catalytic machinery. In the MEROPS database, peptidases are classified into more than 220 families and 40 clans [27] with four primary types of proteases: serine proteases, cysteine proteases, aspartate proteases, and metalloproteases. Cysteine proteases employ a catalytic cysteine residue as a nucleophile to attack the carbonyl carbon atom of peptide bond, often with an aid of a neighboring histidine residue. Our present results suggest that the catalytic machineries for cleaving glycosidic bonds may be more diverse than previously considered. However, we do not exclude a possibility of a normal 'two carboxylate' reaction mechanism because the distance between Glu322 and Glu338 (4.9 Å) is within a range of usual retaining GHs. Further studies (e.g., determination of a covalent intermediate structure) are required to validate the possibility of an unprecedented GH mechanism.

Acknowledgments

We thank the staff of the Photon Factory and SPring-8 for the X-ray data collection and Japan Advanced Plant Science Network for ICP-OES measurements. Beam time at SPring-8 was supported by the Priority Program for Disaster-Affected Quantum Beam Facilities. Computational time was provided by the Texas Advanced Computing Center Stampede cluster under the National Science Foundation Extreme Science and Engineering Discovery Environment, Grant number MCB-090159 and by the NREL Computational Science Center. This work was supported by Japan Society for the Promotion of Science KAKENHI Grant 24380053, Platform for Drug Discovery, Informatics, and Structural Life Science from MEXT, Japan, the United States Department of Energy BioEnergy Technologies Office, and the NREL Laboratory Directed Research and Development program.

Appendix A. Supplementary data

Supplementary data associated with this article can be found, in the online version, at http://dx.doi.org/10.1016/j.bbrc.2014.03.096.

References

[1] B.L. Cantarel, P.M. Coutinho, C. Rancurel, T. Bernard, V. Lombard, B. Henrissat, The Carbohydrate-Active EnZymes database (CAZy): an expert resource for glycogenomics, Nucleic Acids Res. 37 (2009) D233–238.
[2] M.J. Kieliszewski, A.M. Showalter, J.F. Leykam, Potato lectin: a modular protein sharing sequence similarities with the extensin family, the hevein lectin family, and snake venom disintegrins (Platelet aggregation inhibitors), Plant J. 5 (1994) 849–861.
[3] M.J. Kieliszewski, D.T. Lamport, Extensin: repetitive motifs, functional sites, post-translational codes, and phylogeny, Plant J. 5 (1994) 157–172.
[4] S.M. Velasquez, M.M. Ricardi, J.G. Dorosz, P.V. Fernandez, A.D. Nadra, L. Pol-Fachin, J. Egelund, S. Gille, J. Harholt, M. Ciancia, H. Verli, M. Pauly, A. Bacic, C.E. Olsen, P. Ulvskov, B.L. Petersen, C. Somerville, N.D. Iusem, J.M. Estevez, *O*-glycosylated cell wall proteins are essential in root hair growth, Science 332 (2011) 1401–1403.
[5] D. Ashford, N.N. Desai, A.K. Allen, A. Neuberger, M.A. O'Neill, R.R. Selvendran, Structural studies of the carbohydrate moieties of lectins from potato (*Solanum tuberosum*) tubers and thorn-apple (*Datura stramonium*) seeds, Biochem. J. 201 (1982) 199–208.
[6] D. Mohnen, Pectin structure and biosynthesis, Curr. Opin. Plant Biol. 11 (2008) 266–277.
[7] Y. Matsubayashi, Post-translational modifications in secreted peptide hormones in plants, Plant Cell Physiol. 52 (2011) 5–13.
[8] M. Ogawa-Ohnishi, W. Matsushita, Y. Matsubayashi, Identification of three hydroxyproline *O*-arabinosyltransferases in *Arabidopsis thaliana*, Nat. Chem. Biol. 9 (2013) 726–730.
[9] K. Fujita, S. Sakamoto, Y. Ono, M. Wakao, Y. Suda, K. Kitahara, T. Suganuma, Molecular cloning and characterization of a β-L-Arabinobiosidase in *Bifidobacterium longum* that belongs to a novel glycoside hydrolase family, J. Biol. Chem. 286 (2011) 5143–5150.
[10] K. Fujita, Y. Takashi, E. Obuchi, K. Kitahara, T. Suganuma, Characterization of a novel β-L-Arabinofuranosidase in *Bifidobacterium longum*: functional elucidation of A DUF1680 protein family member, J. Biol. Chem. 289 (2014) 5240–5249.
[11] Z. Zhu, M. He, C.-H. Huang, T.-P. Ko, Y.-F. Zeng, Y.-N. Huang, S. Jia, F. Lu, J.-R. Liu, R.-T. Guo, Crystallization and preliminary X-ray diffraction analysis of a novel β-L-arabinofuranosidase (HypBA1) from *Bifidobacterium longum*, Acta Crystallogr. F Struct. Biol. Cryst. Commun. (2014) in press.
[12] S. Kaeothip, A. Ishiwata, T. Ito, S. Fushinobu, K. Fujita, Y. Ito, Preparation of *p*-nitrophenyl β-L-arabinofuranoside as a substrate of β-L-arabinofuranosidase, Carbohydr. Res. 382 (2013) 95–100.
[13] M.J. Frisch, G.W. Trucks, H.B. Schlegel, G.E. Scuseria, M.A. Robb, J.R. Cheeseman, G. Scalmani, V. Barone, B. Mennucci, G.A. Petersson, Gaussian 09, Revision B.01, Gaussian Inc., Wallingford, CT, 2010.
[14] V. Barone, M. Cossi, Quantum calculation of molecular energies and energy gradients in solution by a conductor solvent model, J. Phys. Chem. A 102 (1998) 1995–2001.
[15] M. Cossi, N. Rega, G. Scalmani, V. Barone, Energies, structures, and electronic properties of molecules in solution with the C-PCM solvation model, J. Comput. Chem. 24 (2003) 669–681.
[16] R.-Z. Liao, W. Thiel, On the effect of varying constraints in the quantum mechanics only modeling of enzymatic reactions: the case of acetylene hydratase, J. Phys. Chem. B 117 (2013) 3954–3961.
[17] J.M. Goodman, M.A. Silva, QRC: a rapid method for connecting transition structures to reactants in the computational analysis of organic reactivity, Tetrahedron Lett. 44 (2003) 8233–8236.
[18] M.A. Silva, J.M. Goodman, Aziridinium ring opening: a simple ionic reaction pathway with sequential transition states, Tetrahedron Lett. 46 (2005) 2067–2069.
[19] A.H. Conner, L. Anderson, The tautomerization and mutarotation of β-L-arabinopyranose. Participation of both furanose anomers, Carbohydr. Res. 25 (1972) 107–116.
[20] Y. Nakamichi, Y. Maruyama, B. Mikami, W. Hashimoto, K. Murata, Structural determinants in streptococcal unsaturated glucuronyl hydrolase for recognition of glycosaminoglycan sulfate groups, J. Biol. Chem. 286 (2011) 6262–6271.
[21] T. Itoh, A. Ochiai, B. Mikami, W. Hashimoto, K. Murata, Structure of unsaturated rhamnogalacturonyl hydrolase complexed with substrate, Biochem. Biophys. Res. Commun. 347 (2006) 1021–1029.
[22] E. Ficko-Blean, C.P. Stuart, A.B. Boraston, Structural analysis of CPF_2247, a novel alpha-amylase from *Clostridium perfringens*, Proteins 79 (2011) 2771–2777.
[23] M.R. Stam, E. Blanc, P.M. Coutinho, B. Henrissat, Evolutionary and mechanistic relationships between glycosidases acting on α- and β-bonds, Carbohydr. Res. 340 (2005) 2728–2734.
[24] D.S. Alud, Zinc coordination sphere in biochemical zinc sites, Biometals 14 (2011) 271–313.
[25] S.A.K. Jongkees, S.G. Withers, Unusual enzymatic glycoside cleavage mechanisms, Acc. Chem. Res. 47 (2014) 226–235.
[26] T.V. Vuong, D.B. Wilson, Glycoside hydrolases: catalytic base/nucleophile diversity, Biotechnol. Bioeng. 107 (2010) 195–205.
[27] N.D. Rawlings, A.J. Barrett, A. Bateman, MEROPS: the database of proteolytic enzymes, their substrates and inhibitors, Nucleic Acids Res. 40 (2012) D343–350.